J. Meas. Sci. Instrum., 2025, 16(3): 350-358. http://jmsi.publish.founderss.cn
DOI: 10.62756/jmsi.1674-8042.2025034 jmsi@nuc.edu.cn

Adaptive fringe projection method for high dynamic range objects measurement

LI Yifan, FU Luhua, SUN Changku, WANG Peng*

State Key Laboratory of Precision Measurement Technology and Instruments, Tianjin University, Tianjin 300072

***Corresponding author:** WANG Peng (wang_peng@tju.edu.cn)

Received: November 25, 2024 **Revised:** December 27, 2024 **Accepted:** February 28, 2025

Abstract: Grating fringe projection 3D measurement techniques are extensively applied in various fields. However, in high dynamic range scenarios with significant surface reflectivity variations, uneven greyscale distribution may lead to phase errors and poor reconstruction results. To address this problem, an adaptive fringe projection method is introduced. The method involves projecting two sets of dark and light fringes onto the object, enabling the full-field projection intensity map to be generated adaptively based on greyscale analysis. First, dark fringes are projected onto the object to extend exposure time as long as possible without causing overexposure in the image. Subsequently, bright fringes are projected under the same exposure settings to detect overexposed pixels, and the greyscale distribution of these overexposed points from the previous dark fringe projection is analyzed to calculate the corresponding projection intensities. Finally, absolute phase information from orthogonal fringes is used for coordinate matching, enabling the generation of adaptive projection fringe patterns. Experiments on various high dynamic range objects show that compared to conventional fringe projection binocular reconstruction method, the proposed algorithm achieves complete reconstruction of high dynamic range surfaces and shows robust performance against phase calculation errors caused by overexposure and low modulation.

Key words: fringe projection; 3D measurement; high dynamic range; adaptive fringe; multi-frequency phase shift

0 Introduction

Fringe projection 3D measurement is an important method in non-contact 3D measurement technology[1]. With its advantages of a simple system, fast measurement speed, high accuracy and resolution, it is widely applied in areas such as industrial inspection, reverse engineering, medical diagnosis, and cultural heritage preservation[2-6]. This method involves using a projector to cast fringe patterns onto the surface of the target, capturing the deformed fringes with cameras, and utilizing calibration parameters to reconstruct the 3D contour of the object[7]. Despite its benefits, this method faces certain challenges. For example, due to the limited grayscale intensity range of the camera, the object with high dynamic range, which refers to scenes or surfaces containing both very bright and very dark areas simultaneously, often struggles to achieve high-quality reconstruction. The main reason is overexposure in the captured images, where bright areas lose detail and signal-to-noise ratio (SNR) is low, which affects the clarity of dark regions.

In high dynamic range scenarios, factors such as the color and material of the measured surface cause significant variations and uneven distribution in reflectivity. Under a fixed light source, this leads to considerable differences in the distribution of reflected light intensity. Consequently, the greyscale of the fringe image captured in a single exposure becomes uneven, with some areas appearing excessively bright or dark, leading to missing or highly inaccurate phase information. Ultimately, the accuracy of the reconstruction results is affected. To overcome the challenges in high dynamic range surface fringe projection reconstruction, researchers have explored various strategies[8,9]. These solutions can be classified into three categories, adjusting exposure time, modifying projection patterns, and integrating additional hardware. The first approach is to adjust the camera's exposure time. Zhang et al.[10] achieved full reconstruction by fusing images captured at different exposure times, though this method is complex and relies heavily on experience. Rao et al.[11] introduced an approach that automatically calculates exposure time based on pixel modulation, simplifying the reconstruction process. Wang et al.[12] estimated a suitable exposure time

© The Author(s) 2025. Published by Publishing Center of North University of China. The articles published in this open access journal are distributed under the terms of the Creative Commons Attribution 4.0 International License (http://creativecommons.org/licenses/by/4.0/), which permits use, distribution and reproduction in any medium, provided the original work is properly cited.

interval using two sets of fringes, then selected an optimal exposure time and captured images using high-speed projection technology. This method eliminates unnecessary image acquisition, ensuring the fringe validity and improving measurement efficiency.

Another strategy is to modify the projection fringe patterns. Waddington and Kofman[13] developed a maximum input grey level algorithm to adapt to changing ambient light conditions. However, it struggles to maintain a high SNR in darker regions and is relatively inefficient for measurements. Chen et al. [14] determined the optimal projection intensity for each pixel by casting a series of uniform grey-level patterns onto the object, and then utilized orthogonal color fringes to convert the pixel coordinate system and generate the optimal projection fringe patterns. This method requires manually selecting the number of grey-level patterns to balance measurement accuracy and efficiency. Liu et al.[15] employed a 255 grey-level pattern to mark saturated regions and a lower-intensity uniform image to calculate the optimal projection intensities for the pixels in these areas. Although this approach reduces the number of projected patterns, it slightly compromises measurement accuracy.

Moreover, measurement accuracy can be enhanced by integrating extra cameras, projectors, or polarizing filters[16-19]. However, these methods require additional hardware, increasing system complexity and raising the requirements for setup and calibration.

Although notable progress has been made, the shortcomings of existing methods still constrain the applicability. To overcome these limitations and improve the reconstruction of high dynamic range surface objects, this article introduces an adaptive fringe projection method. This approach eliminates pre-calibration requirements, determining all projection intensities using only two sets of dark and light fringes. By matching coordinates with the assistance of low-brightness orthogonal fringes, it generates adaptive projection patterns. Experimental results show that this method allows cameras to capture high-quality images, significantly improving reconstruction completeness and accuracy.

1 Principle

1.1 System response relationship and phase calculation

The projection-reflection model for a standard scene is initially introduced. In the absence of high dynamic range characteristics, the formation of a fringe image in the camera involves three steps: fringe pattern projection by the projector, reflection from the object, and image capture by the camera. As illustrated in Fig. 1, the light entering the cameras can be divided into three main types: projector light reflected off the object ρI^p; ambient light reflected from the object ρI^a; and ambient light directly entering the camera I^b. Taking into account the noise generated by the camera sensor during imaging I^n, the intensity of the pixels in the captured fringe image $I^c(x,y)$ can be expressed as

$$I^c(x,y)=\gamma t\left[\rho(x,y)I^p(u,v)+\rho(x,y)I^a+I^b\right]+I^n, \tag{1}$$

where ρ denotes the reflectivity of the object's surface, γ is the camera's sensitivity, and t represents the exposure time. In a dark environment, the intensity of the projector's fringes is much higher than that of ambient light, allowing I^a and I^b to be approximated as zero. Noise effects will be addressed later and are temporarily disregarded here. Under these conditions, Eq. (1) is simplified to

$$I^c(x,y)=\gamma t\rho(x,y)I^p(u,v). \tag{2}$$

Eq. (2) indicates that if the camera parameters and the object's position remain unchanged throughout the measurement process, meaning γ, t and $\rho(x,y)$ are fixed, the intensity of the camera image is directly proportional to the projection intensity.

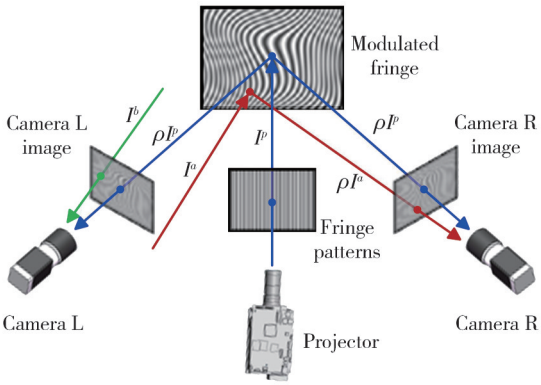

Fig. 1 Schematic of binocular system and light composition

However, when the surface exhibits high dynamic range characteristics, Eq. (2) is no longer valid. As shown in Fig. 2, overexposure occurs in the red-boxed area of a measurement image due to the object's high reflectivity. In such cases, the pixel greyscale value is no longer proportional to the projection intensity and is instead limited to a maximum of 255. In the yellow box, the object's low reflectivity causes minimal fringe variation, resulting in excessively low modulation. Both overexposure and low modulation lead to phase-solving errors, ultimately impacting the measurement results. To ensure the camera captures high-quality fringe images, we propose a method that generates adaptive projection fringes for different sub-

areas. Low-brightness fringes are projected onto high-reflective areas, while high-brightness fringes are applied to low-reflective areas. This approach aims to enhance reconstruction outcomes and improve measurement accuracy.

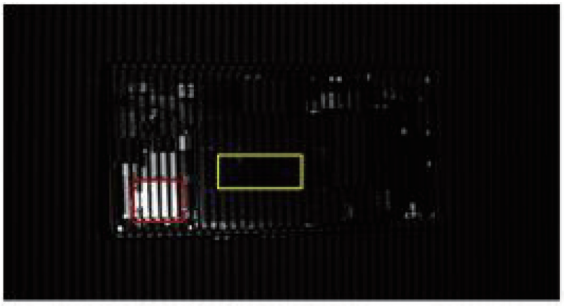

Fig. 2 High dynamic range object measurement fringe image

In surface structured light 3D measurement, phase-shift encoding effectively mitigates the influence of ambient light while ensuring high phase resolution accuracy. By projecting $N(N \geqslant 3)$ phase-shifted grating fringe patterns onto the object, the cameras capture modulated images, which are used to compute the wrapped phase for each pixel. The intensity of the fringe images recorded by the camera is calculated by

$$I_k^c(x,y) = A(x,y) + B(x,y)\cos\left[\varphi(x,y) + \frac{2\pi k}{N}\right], \quad (3)$$

where $k = 0, 1, \cdots, N-1$; $A(x,y)$ and $B(x,y)$ are the average light intensity and fringe amplitude, respectively; and $\varphi(x,y)$ denotes the initial phase value. In this paper, four-step phase-shifting method is used, with a phase difference of $\pi/2$ between consecutive images. The wrapped phase $\varphi(x,y)$ is calculated by

$$\varphi(x,y) = \arctan\left[\frac{I_1^c(x,y) - I_3^c(x,y)}{I_0^c(x,y) - I_2^c(x,y)}\right]. \quad (4)$$

Since the arctangent function constrains the phase $\varphi(x,y)$ within $(-\pi,\pi)$, resulting in periodic variations, the three-frequency heterodyne method is applied for phase unwrapping. Fringe frequencies of 81, 80, and 72 are selected to obtain the monotonic absolute phase.

In high dynamic range scenes, calculating the wrapped phase is particularly challenging. When overexposure occurs, the maximum grey level of 255 no longer reflects the true brightness of the scene, resulting in incorrect or missing phase values. Moreover, since the phase error is given by

$$\Delta\varphi = \frac{2}{NB}\sum_{k=0}^{N}\sin\left(\varphi + \frac{2\pi k}{N}\right)\Delta A_n, \quad (5)$$

where ΔA_n is random noise[20], underexposure leads to low fringe modulation, which amplifies the error. Therefore, capturing high-quality fringe images is crucial for minimizing errors in the wrapped phase calculation.

1.2 Adaptive fringe projection algorithm

1.2.1 Determination of adaptive projection intensity

The conventional adaptive fringe projection method generates optimal fringe patterns by calculating the ideal projection grey value for each pixel in the camera image. This ensures high modulation in the captured images, leading to high-quality phase calculation results. However, for large image sizes with a high pixel count, computing the optimal projection intensity for every pixel becomes time-consuming. This results in a complex greyscale composition for the final optimal fringe patterns, making the process cumbersome and lowering measurement efficiency. To streamline the projection process, studies have shown that if the industrial camera's SNR exceeds 30 dB, and the maximum greyscale value of fringe images is 100 or more, variations in the greyscale range have minimal impact on phase calculation errors[21]. Therefore, calculating optimal intensity for each pixel is not essential. Instead, a single projection intensity can be used for all pixel points in the camera image with grey values above a pre-defined threshold.

In contrast to approaches that compute the optimal projection intensity for every pixel, our method segments the modulated image into multiple regions. By determining the projection intensity for each region, the high dynamic range object can be reconstructed more completely. Furthermore, an adaptive method is introduced to determine the intensity of the fringes. This method generates global projection intensity maps using only two sets of light and dark fringes, eliminating the need for a complex pre-calibration process. First, a set of dark fringe patterns are projected, and the maximum greyscale value I_{p1} is recorded. This value can be adjusted based on the object's surface properties. The exposure time of the camera is extended without saturating the pixels in the captured images, and this time remains fixed throughout subsequent measurements. Considering the noise generated during camera imaging and the actual experimental conditions, pixels with a greyscale exceeding 250 are treated as saturated. The maximum grey level of each pixel in the images is calculated and visualized as the base map $Img_1(x,y)$. Then, a set of bright fringe patterns is projected, with sinusoidal pattern greyscales mapped to the range of 0—240, defining I_{p0} as 240. The captured image is used to generate the maximum greyscale map $Img_0(x,y)$. For the unsaturated pixels in this map, the fringe

modulation is maximized, making the corresponding projection intensity I_{p0} optimal. For saturated pixels, additional calculations are required to determine the projection intensity.

To obtain the greyscale distribution of the overexposed pixels in $Img_0(x,y)$ in the base map $Img_1(x,y)$, a mask $M(x,y)$ is constructed, which is defined as

$$M(x,y)=\begin{cases}1, \ \mathrm{Img}_0(x,y)>250,\\ 0, \ \mathrm{Img}_0(x,y)\leqslant 250.\end{cases} \tag{6}$$

Subsequently, a grey histogram is generated for the pixels where $M(x,y)$ equals 1 in $Img_1(x,y)$ and the maximum and minimum grey level values $I_{\max}$ and $I_{\min}$, are determined for further analysis. A grey level threshold I_{th} is set, and pixels above this threshold are acceptable. In contrast, pixels below this threshold require brighter fringes to enhance their modulation and improve phase calculation accuracy. This means that the usable pixel greyscale interval is I_{th} to 250. The strategy for the automatic determination of the projection intensity is analyzed in the following.

Since the exposure time is maximized on the basis that the image is not overexposed, in most cases $I_{\max}>I_{\mathrm{th}}$, indicating that at the projected intensity of I_{p1}, there are some usable pixels, I_{p1} is the lowest projected intensity, and the lowest grey value of the usable pixels in the histogram at that intensity I'_{p1} is I_{th}. For points with greyscale less than or equal to I_{th}, new projection intensities have to be calculated further. In order to have the maximum number of pixels that meet the requirement at the next brighter projection intensity I_{p2}, the points with current grey value of I_{th} are to be made to 250. From the linear relationship between the image greyscale and projection intensity, the following equation can be obtained as

$$\frac{I_{p2}}{I_{p1}}=\frac{250}{I_{\mathrm{th}}}. \tag{7}$$

Defining $const=250/I_{\mathrm{th}}$, we have $I_{p2}=I_{p1}\cdot const$. At this point in the histogram, the highest grey value of the usable pixels is I_{th} and the lowest grey value I'_{p2} is $I_{\mathrm{th}}/const$. Similarly, the next projection intensity I_{p3} satisfies $I_{p3}=I_{p2}\cdot const=I_{p1}\cdot const^2$, and $I'_{p3}=I_{\mathrm{th}}/const^2$. For the minimum grey value $I_{\min}$ in the histogram, the corresponding projection intensity I_{pm} satisfies the following equation in order to make it meet the requirement of

$$\frac{I_{pm}}{I_{p1}}=\frac{I_{\mathrm{th}}}{I_{\min}}. \tag{8}$$

Iteratively calculating the projection intensity $I_{pn}=I_{p1}\cdot const^{n-1}$ and the corresponding $I_{pn}'=I_{\mathrm{th}}/const^{n-1}$, the calculation ends when $I_{pn}\geqslant I_{pm}$ or $I_{pn}\geqslant 240$. From this, all the required projection intensities, from dark to light, can be automatically calculated as I_{p1}, I_{p2}, $\cdots$, $I_{p(n-1)}$, I_{pm}, and I_{p0}. The process is illustrated in Fig.3.

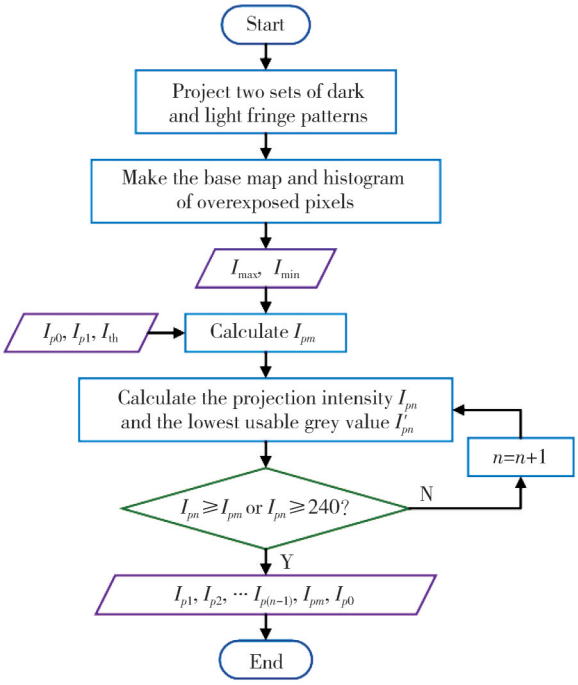

Fig. 3 Flow chart of determining adaptive projection intensity

1.2.2 Generation of adaptive projection fringe patterns

Once the projection intensities are determined, adaptive fringe patterns need to be generated regionally so that the cameras can capture high-quality images in a single exposure. This is achieved by establishing the relationship between the camera's pixel coordinate system and the projector's pixel coordinate system. Two sets of low-brightness vertical and horizontal patterns are projected onto the object, and the corresponding projector pixel coordinates are identified by solving the absolute phase in both directions. Although single-intensity projection is insufficient for high-quality reconstruction due to the object's large dynamic range, it suffices for establishing coordinate correspondence. The absolute phases of a point (x,y) in the camera image along the horizontal and vertical directions are $\Phi_h(x,y)$ and $\Phi_v(x,y)$ respectively, and their projector coordinates are obtained as

$$\begin{cases}u=\dfrac{V\Phi_v(x,y)}{2\pi T}+\dfrac{V}{2},\\ v=\dfrac{H\Phi_h(x,y)}{2\pi T}+\dfrac{H}{2},\end{cases} \tag{9}$$

where V and H are the width and height of the projector image, T represents the maximum number of fringe periods.

In the previous section, all the required projection

intensities were derived. Additionally, the base map pixels corresponding to each projection intensity can be determined based on the grey value. Accordingly, the mask $M_i^c(x,y)$ corresponding to the camera image pixels for each projection intensity can be defined as

$$M_i^c(x,y)=\begin{cases}1, & Img_1(x,y)>I_{p1}',\\ 0, & \text{else},\end{cases}\quad (i=1);$$

$$M_i^c(x,y)=\begin{cases}1, & I_{pi}'<Img_1(x,y)<I_{p(i-1)}',\\ 0, & \text{else},\end{cases}\quad (i=2,3,\cdots,n-1). \tag{10}$$

Subsequently, the mask $M_i^p(u,v)$ for each light intensity in the projector fringe pattern corresponding to $M_i^c(x,y)$ is obtained with the help of Eq. (9). The final adaptive patterns can be obtained by fusing the fringe maps with different intensities using mask $M_i^p(u,v)$ and filling the remaining part with maps with intensity I_{p0}. These patterns allow for projecting darker fringes onto highly reflective areas to prevent pixel saturation, while brighter fringes are projected onto darker areas to maintain proper modulation and phase resolution accuracy.

In conclusion, the steps of the adaptive fringe projection algorithm proposed in our work are as follows:

1) Project a set of dark fringe patterns, determine the maximum exposure time at which the camera image remains unsaturated, calculate the maximum grey level of each pixel, and generate the base map $Img_1(x,y)$.

2) Project a set of bright fringe patterns, create a mask for saturated pixels $M(x,y)$, and generate the grey histogram for the corresponding pixels in the base map.

3) Based on the proposed adaptive projection intensity strategy, determine all the projection intensities I_{p1}, I_{p2}, $\cdots$, $I_{p(n-1)}$, I_{pm}, I_{p0}.

4) Create masks for each projection intensity in the camera image, and transform the coordinates by projecting vertical and horizontal fringes to obtain corresponding masks in the projector image $M_i^p(u,v)$.

5) Fuse the fringe patterns for each intensity to generate adaptive projection patterns, followed by performing 3D reconstruction of the object.

2 Experiments

The binocular experimental system used in our work is shown in Fig. 4. The projector is a DLP4710 from TI with a resolution of 1 920×1 080. Both cameras are Basler acA4096-30um black and white models with a resolution of 4 096×2 160 and a typical SNR of 40.1 dB, paired with C11-2520-12M-P f25mm fixed-focus lenses. The system has a measurement distance of approximately 400 mm and a measurement range of about 210 mm×110 mm.

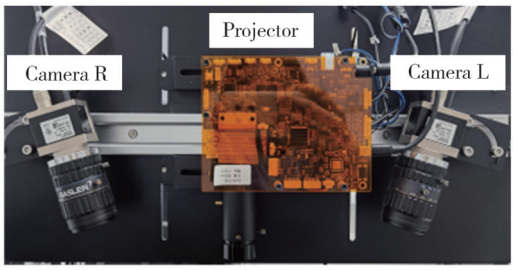

Fig. 4 Binocular experiment system

To evaluate the effectiveness of the proposed algorithm, high dynamic range surface objects were selected for reconstruction. As shown in Fig. 5, a calibration board with a wide range of surface colours and a mobile phone part with complex surface structures, containing various materials and colours, were chosen as the test objects.

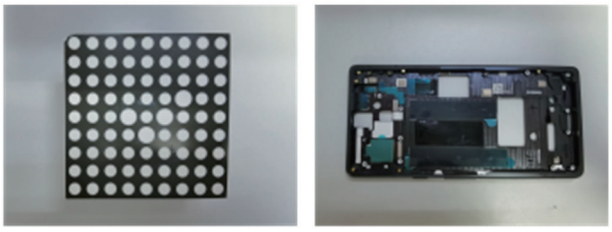

(a) Calibration board (b) Mobile phone part

Fig. 5 High dynamic range surface objects

The calibration board was first measured using the traditional method of projecting a single intensity of fringe. When projecting fringe patterns with a maximum intensity of 240, the images captured by the cameras are shown in Fig. 6(a) and (b). Fig. 6(c) and (d) show the camera images when projecting fringes with a maximum intensity of 60.

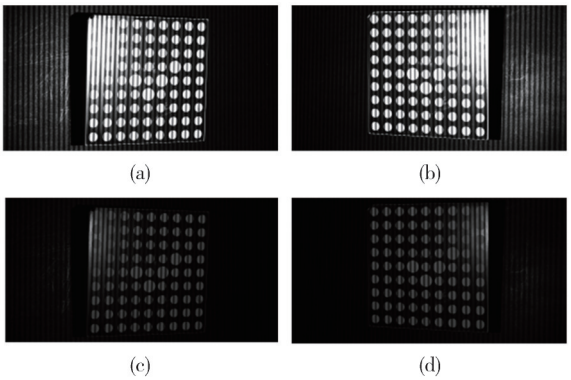

(a) (b) (c) (d)

Fig. 6 Calibration board images by traditional method. (a)–(b) Images captured by left and right cameras at the projection intensity of 240, and (c)–(d) Images captured by left and right cameras at the projection intensity of 60

Fig. 7 shows the greyscale values of some pixels in a row of the left camera image at two projection intensities.

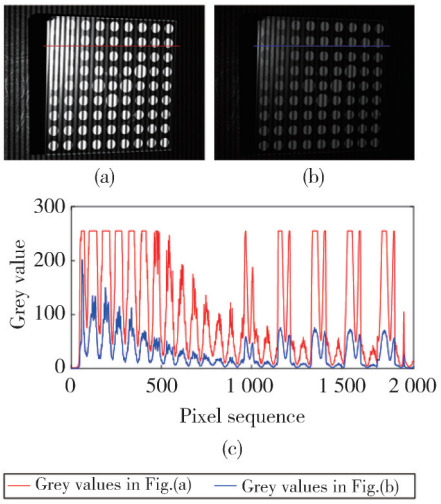

Fig. 7 Grayscale values of pixels. (a)-(b) Pixels extracted from left camera at two projection intensities, and (c) Pixel grey value

When using the method proposed in our work, a set of dark fringe patterns with $I_{p1}=40$ was firstly projected, and the exposure time was adjusted to 17 000 μs, and it was found that no saturation occurred in both left and right camera images, so it was determined to be the exposure time for subsequent measurements. The bright fringe patterns with $I_{p0}=240$ were then projected, and the histogram of the pixels in the base map that were overexposed at this time was made, as shown in Fig.8. The minimum and maximum greyscale values were 36 and 246 in the left image, and 37 and 212 respectively in the right image, so $I_{\max}$ was 246, $I_{\min}$ was 36. For ease of calculation, I_{th} was set to 125, and I_{pm} was calculated to be 140. The results of the adaptive projection intensities are listed in Table 1. The final projection intensities are 40, 80, 140 and 240.

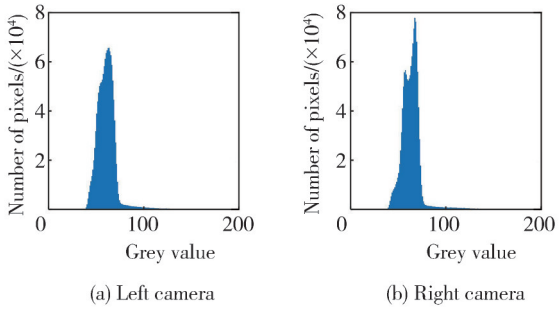

Fig. 8 Histogram of calibration board

Table 1 Adaptive projection intensity calculations

n	I_{pn}	I'_{pn}
2	80	63
3	160	32

Subsequently, to obtain the coordinate correspondence between the cameras and the projector, two sets of orthogonal fringe patterns with darker intensity are projected to the object. Taking the left camera as an example, the captured vertical and horizontal images are shown in Fig.9(a) and (c), and the absolute phases are shown in Fig.9(b) and (d). The final adaptive projection patterns are shown in Fig.10, and the camera images are shown in Fig.11. It can be seen that the new patterns can effectively avoid saturation in the brighter regions, while keeping the modulation and SNR high in the darker regions.

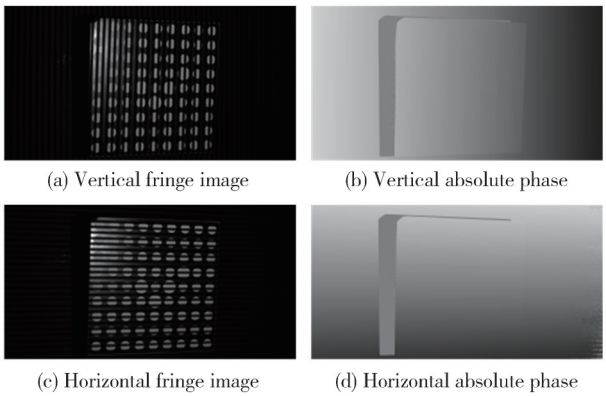

Fig. 9 Coordinate correspondence result

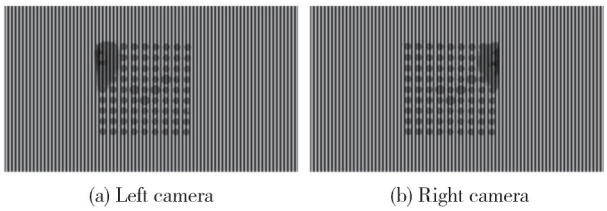

Fig. 10 Calibration board adaptive projection pattern

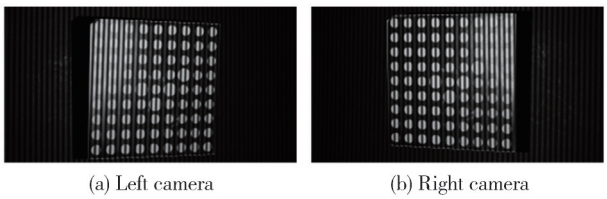

Fig. 11 Camera images

Fig.12 compares the reconstruction results of the three methods. Fig. 12(a) and (b) show the results when projecting single bright and dark fringes. It is evident that pixel saturation in the camera as well as low modulation and SNR leads to incomplete reconstructions or significant reconstruction errors. Conventional methods using a single projection intensity are unable to achieve a complete and high-quality reconstruction of high dynamic range surface. Both the method in Ref.[21] and the method proposed in our work are capable of achieving a complete reconstruction of the calibration board.

Fig. 13 compares the phase resolution results from images captured by the left camera using traditional methods and the proposed method. The shaded portion cannot be successfully resolved. When the intensity is too bright, the phase of the saturated region is calculated

incorrectly, conversely, there is a lot of noise. When the adaptive fringe patterns are projected, the correct phase resolution can be achieved for the whole region at which the object is located.

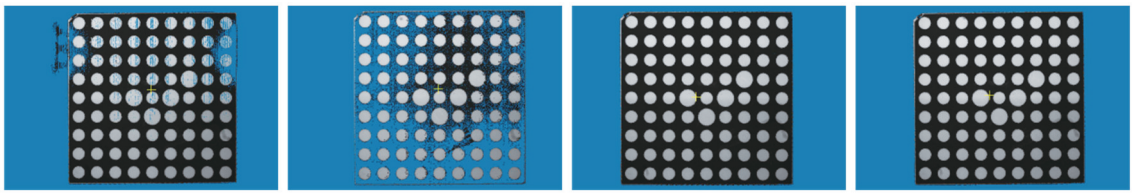

(a) High exposure (b) Low exposure (c) Method in Ref.[21] (d) Proposed method

Fig. 12 Comparison of reconstruction results

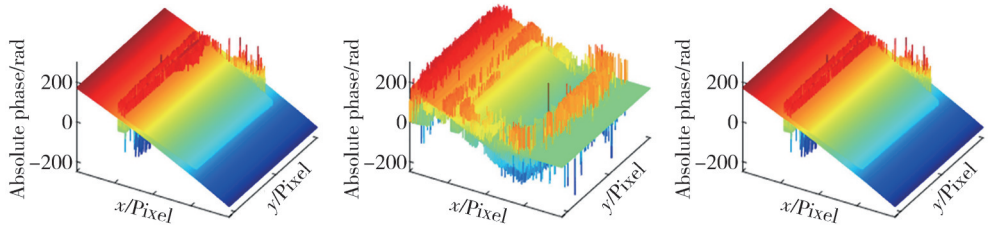

(a) Bright patterns (b) Dark patterns (c) Adaptive patterns

Fig. 13 Comparison of phase resolution results

The surface of the second object, a mobile phone part, is more complex than the calibration board, and Fig. 14 shows the camera images obtained from a single exposure. When using the proposed method, the dark fringe with $I_{p1}=20$ is first projected and the camera exposure time is 8 500 μs. The histogram is shown in Fig. 15, with $I_{\max}=244$ and $I_{\min}=14$. Specifying $I_{\text{th}}=125$, I_{pm} is worked out to be 178. The calculation of the projection intensities is listed in Table 2, so 6 different intensities are needed to measure this part, which are 20, 40, 80, 160, 178 and 240. The final fringe patterns and camera images are shown in Fig. 16.

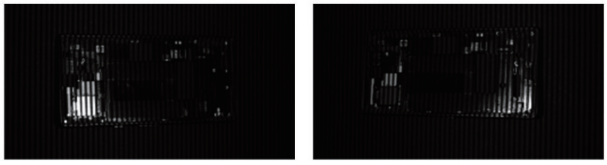

(a) Left camera (b) Right camera

Fig. 14 Mobile phone traditional method images

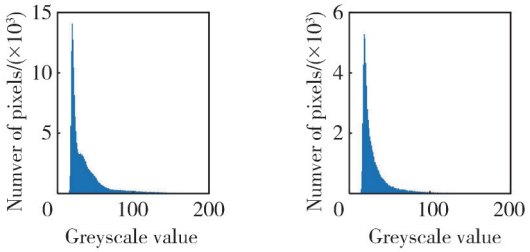

(a) Left camera (b) Right camera

Fig. 15 Histogram of mobile phone part

Table 2 Adaptive projection intensity calculations

n	I_{pn}	I'_{pn}
2	40	63
3	80	32
4	160	16
5	320	—

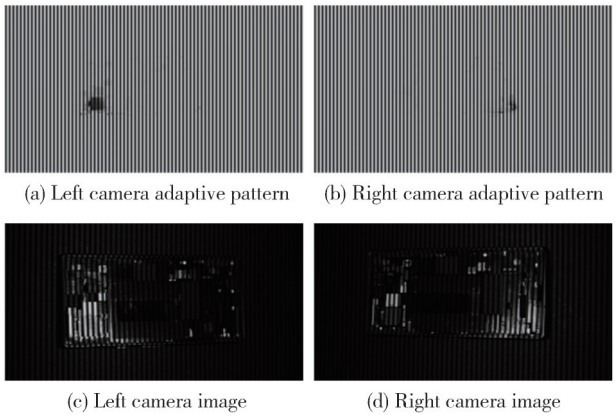

(a) Left camera adaptive pattern (b) Right camera adaptive pattern

(c) Left camera image (d) Right camera image

Fig. 16 Mobile phone adaptive projection pattern and camera images

Fig. 17 compares the reconstruction results of the three methods. When using traditional method, the red boxed area shows point cloud missing due to overexposure from the left camera, while the yellow boxed area fails to reconstruct correctly due to low image brightness, resulting in unsuccessful phase resolution and matching. When using the method from Ref.[21], the reconstruction results in the dark areas show significant improvement, but point cloud missing due to overexposure still exists in the red boxed area. Only the method proposed in this paper is capable of achieving a complete reconstruction of this complex measured object. Fig. 18 presents additional detail images obtained using the proposed method. The absolute phases from the left camera images of the two measurements are compared, as shown in Fig. 19. Except for the shaded regions, the proposed method provides more accurate phase resolution in areas such as the black boxes, effectively complementing the point cloud in both overly bright and dark regions. This significantly enhances the completeness

of the reconstruction. The above experiments demonstrate that the proposed measurement method can effectively measure high dynamic range surface objects, with particularly pronounced advantages when the surface conditions of the objects are complex.

(a) Traditional method (b) Method in Ref.[21] (c) Proposed method

Fig. 17 Reconstruction results

(a) View 1 (b) View 2 (c) View 3

Fig. 18 Detail images

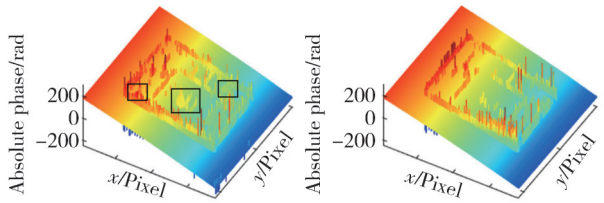

(a) Use single intensity patterns (b) Use adadtive patterns

Fig. 19 Comparison of phase resolution results

Fig. 20 shows the measurement results for other high dynamic range surface objects encountered in everyday life. The first row presents the reconstruction results using traditional methods, while the second row displays the results of the proposed method. It can be observed that the missing parts in the red boxes have been improved. Objects with different materials and colors are successfully reconstructed, further validating the effectiveness of the method proposed in this paper.

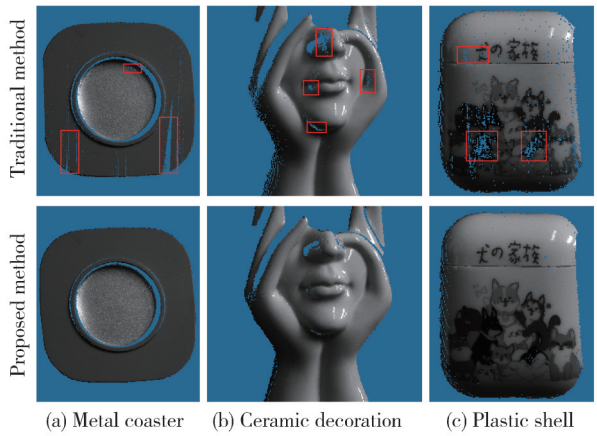

(a) Metal coaster (b) Ceramic decoration (c) Plastic shell

Fig. 20 Point cloud for other objects

3 Conclusions

To address the challenges of measuring high dynamic range objects with fringe projection 3D measurement techniques, this paper proposes an improved adaptive fringe projection method. By projecting two sets of dark and light fringe patterns and analyzing pixel greyscale values, the required projection intensities are automatically calculated. Adaptive projection fringes are then generated based on the correspondence between camera and projector pixels. Compared to existing methods, this approach simplifies the process and eliminates the need for complex calculations. Experimental results demonstrate that this method significantly improves phase resolution accuracy and ensure the integrity of the reconstructed point cloud. It also performs well when dealing with complex objects, enabling effective measurement of high dynamic range objects.

Acknowledgement

This work was supported by the Science and Technology Program Project of Tianjin (No. 24ZXZSSS00300).

Declaration of conflicting interests

The authors have no conflict of interests related to this publication.

References

[1] ZUO C, FENG S J, HUANG L, et al. Phase shifting algorithms for fringe projection profilometry: A review. Optics and Lasers in Engineering, 2018, 109: 23-59.

[2] HU P Y, YANG S M, ZHENG F H, et al. Accurate and dynamic 3D shape measurement with digital image correlation-assisted phase shifting. Measurement Science and Technology, 2021, 32(7): 075204.

[3] SUN J H, ZHANG Q Y. A 3D shape measurement method for high-reflective surface based on accurate adaptive fringe projection. Optics and Lasers in Engineering, 2022, 153: 106994.

[4] LI M H, CAO Y P, WU H T. Three-dimensional reconstruction for highly reflective diffuse object based on online measurement. Optics Communications, 2023, 533: 129276.

[5] LIU Z L, LI M Y, LU X Y, et al. On-machine detection technology and application progress of high dynamic range fringe structured light. Chinese Optics, 2024, 17(1): 1-18.

[6] WANG P, ZHANG X, SUN C K, et al. A method for obtaining complete point cloud of tongue surface based on fringe projection trinocular system. Journal of Measurement Science and Instrumentation, 2024, 15(2): 166-175.

[7] LIU X R, KOFMAN J D. Real-time 3D surface-shape measurement using background-modulated modified

Fourier transform profilometry with geometry-constraint. Optics and Lasers in Engineering, 2019, 115: 217-224.
[8] XIANG S, HUANG Z Z, DENG H P, et al. Adaptive pattern fusion for multi-reflectivity objects in fringe projection profilometry. Optics and Lasers in Engineering, 2024, 174: 107978.
[9] ZHAO X B, ZHANG G Y, LAU D L, et al. Adaptive phase measuring profilometry for robustly detecting saturated pixels. Optics Communications, 2024, 552: 130061.
[10] ZHANG S, YAU S T. High dynamic range scanning technique. Optical Engineering, 2009, 48(3): 033604.
[11] RAO L, DA F P. High dynamic range 3D shape determination based on automatic exposure selection. Journal of Visual Communication and Image Representation, 2018, 50: 217-226.
[12] WANG J H, ZHOU Y G, YANG Y X. A novel and fast three-dimensional measurement technology for the objects surface with non-uniform reflection. Results in Physics, 2020, 16: 102878.
[13] WADDINGTON C J, KOFMAN J D. Modified sinusoidal fringe-pattern projection for variable illuminance in phase-shifting three-dimensional surface-shape metrology. Optical Engineering, 2014, 53(8): 084109.
[14] CHEN C, GAO N, WANG X J, et al. Adaptive pixel-to-pixel projection intensity adjustment for measuring a shiny surface using orthogonal color fringe pattern projection. Measurement Science and Technology, 2018, 29(5): 055203.
[15] LIU Y Z, FU Y J, CAI X Q, et al. A novel high dynamic range 3D measurement method based on adaptive fringe projection technique. Optics and Lasers in Engineering, 2020, 128: 106004.
[16] CHEN C W, XUE J P, ZHANG Q C, et al. Three-dimensional shape measurement of shiny surface based on multi-view equation. Acta Optica Sinica, 2021, 41(22): 92-102.
[17] LIU X H, ZHANG Z H, GAO N, et al. 3D shape measurement of diffused/specular surface by combining fringe projection and direct phase measuring deflectometry. Optics Express, 2020, 28(19): 27561-27574.
[18] FENG S J, ZHANG Y Z, CHEN Q, et al. General solution for high dynamic range three-dimensional shape measurement using the fringe projection technique. Optics and Lasers in Engineering, 2014, 59: 56-71.
[19] ZHU Z M, YOU D D, ZHOU F Q, et al. Rapid 3D reconstruction method based on the polarization-enhanced fringe pattern of an HDR object. Optics express, 2021, 29(2): 2162-2171.
[20] LI Y Y, WU Z J, ZHANG Q C. Phase error compensation technique based on phase-shifting fringe analysis: a review (Invited). Laser & Optoelectronics Progress, 2024, 61(2): 144-163.
[21] MAO C L, LU R S. A new method for 3D shape reconstruction with a high dynamic range surface. Laser & Optoelectronics Progress, 2023, 60(7): 151-160.

面向高动态范围物体测量的自适应条纹投影方法

李依凡，付鲁华，孙长库，王　鹏*

天津大学 精密测试技术及仪器全国重点实验室，天津 300072

摘　要： 目前，光栅条纹投影三维测量技术已在众多领域得到了广泛的应用。然而，对于表面反射率变化较大的高动态范围场景，图像灰度值分布不平衡易导致相位解算出现较大误差，影响重建结果。针对该问题，提出一种自适应条纹投影方法。本方法中，仅需向被测物投影暗亮两组条纹，即可通过灰度分析自适应生成全场投影强度图。首先，向被测场景投影暗条纹，使图像在不过曝的情况下尽量延长曝光时间。其次，在同一曝光时间下投影亮条纹，得到过曝的像素点。对过曝点在投影暗条纹时的灰度分布进行分析以确定对应的投影强度。借助正交条纹的绝对相位信息进行坐标匹配，生成自适应投影条纹。对具有高动态范围特性的不同物体进行实验，结果表明与常规条纹投影双目重建方法相比，本文算法能够实现高动态范围表面物体的完整重建，对过曝和调制度过低等导致的相位解算错误具有较强鲁棒性。

关键词： 条纹投影；三维测量；高动态范围；自适应条纹；多频相移

引用格式： LI Yifan, FU Luhua, SUN Changku, et al. Adaptive fringe projection method for high dynamic range objects measurement. Journal of Measurement Science and Instrumentation, 2025, 16(3): 350-358. DOI: 10.62756/jmsi.1674-8042.2025034